Experimental investigation of the retention factor dependency of eddy dispersion in packed bed columns and relation to knox's empirical model parameters

Desmet, Gert; Song, Huiying; Makey, Devin; Stoll, Dwight R.; Cabooter, Deirdre

Published in:
Journal of Chromatography A

DOI:
10.1016/j.chroma.2020.461339

Publication date:
2020

Experimental investigation of the retention factor dependency of eddy dispersion in packed bed columns and relation to Knox's empirical model parameters

Gert Desmet[(1,*)], Huiying Song[(2)], Devin Makey[(3)], Dwight R. Stoll[(3)], Deirdre Cabooter[(2)]

[(1)]Vrije Universiteit Brussel, Department of Chemical Engineering, Pleinlaan 2, 1050 Brussel, Belgium

[(2)]KU Leuven, Department for Pharmaceutical and Pharmacological Sciences, Pharmaceutical Analysis, Herestraat 49, Leuven, Belgium

[(3)]Department of Chemistry, Gustavus Adolphus College, Saint Peter, Minnesota 56082, United States

[(*)] Corresponding author E-mail: gedesmet@vub.be

Highlights

- Extensive measurement set reveals a systematic k-dependency of eddy dispersion
- Eddy dispersion was determined using novel, CFD-validated Sherwood-expression
- Eddy dispersion data (h_{eddy}) fit well with Knox's empirical eddy dispersion model
- The k-dependency of the exponent and pre-factor of Knox's model is mapped
- A simple mathematical expression to predict h_{eddy} for different k is established

Abstract

We report on a systematic and comprehensive ($0.7 \leq k'' \leq 122$) experimental study of the effect of the zone retention factor k'' on eddy dispersion (h_{eddy}) in packed bed columns for liquid chromatography. The values for h_{eddy} are obtained by subtracting rigorously estimated contributions to the total plate height from longitudinal diffusion (h_B) and the mobile (h_{Cm}) and stationary zone (h_{Cs}) mass transfer resistances. For the first time, h_{Cm}-values are calculated using an expression for the Sherwood-number (Sh) that has been established and validated in the relevant velocity range. Experiments were carried out on both a fully-porous and a core-shell particle column. In both cases, the eddy dispersion systematically decreased with increasing retention factor k'', dropping 0.5 to 0.8 reduced plate height units when going from the lowest to the highest k''. To establish a simple empirical fitting equation that

can represent the observed effects, the widely used power law-based Knox model has been extended to express the dependence of its A- and n-parameters on the retention factor.

Keywords: eddy dispersion; Knox equation; Sherwood; mass transfer; zone retention factor

1. Introduction

Next to longitudinal diffusion, which dominates the low velocity regime of the van Deemter-curve, eddy dispersion is responsible for the largest part of band broadening in packed bed columns used for chromatography [1–3]. Research into its origin, relevance, modelling and potential solutions to suppress its effect has therefore always been an important and recurring topic in the field [4–7]. Historically, the eddy dispersion has been considered as the parameter representing the "goodness of packing", as its original definition relates to the contribution originating from the inevitable difference in length between the multiple parallel through-pores running through a packed bed, which is considered to be a structural property of the packing [8]. Nowadays, based on the general rate model of chromatography [9–11], the eddy dispersion is typically determined as the part of the band broadening that does not originate from the longitudinal diffusion (h_B) or the finite time needed for the mass-transfer to and within the particles (h_{Cm}+h_{Cs}). These are contributions that cannot be dispensed with, while the remaining dispersion must originate from the heterogeneities in the bed, which through some smart engineering, could, at least in theory, be evaded. Mathematically, h_{eddy} is in this case defined as [9,12,13]:

$$h_{eddy}=h-h_B-h_{Cm}-h_{Cs} \tag{1}$$

With:

$$h_B = \frac{B}{\nu_i} = \frac{2}{\nu_i}\frac{D_{eff}}{D_m}(1+k'') \tag{2a}$$

and:

$$h_{Cm} = \frac{1}{3}\frac{k''^2}{(1+k'')^2}\frac{\varepsilon_e}{1-\varepsilon_e}\frac{\nu_i}{Sh} = C_m\nu_i \tag{2b}$$

and:

$$h_{Cs} = \frac{4}{9}\frac{1-\rho^3}{\frac{2}{15}-\frac{2}{3}\rho^3+\frac{6}{5}\rho^5-\frac{2}{3}\rho^6}\frac{k''}{(1+k'')^2}\frac{D_m}{D_{pz}}\nu_i = C_s\nu_i \tag{2c}$$

wherein ν_i is the reduced interstitial velocity (ν_i=u_i.d_p/D_{mol}), ε_e the external porosity, k'' the zone retention factor [11] and D_{pz} the diffusion coefficient prevailing in the porous zone of the particles. Sh is the mobile zone Sherwood number, the dimensionless mass transfer coefficient governing the mass transfer from the mobile zone to the particles [14].

The eddy dispersion is commonly accepted to consist of a multitude of contributions $h_{eddy,j}$, each relating to a different scale j, i.e., to a different transversal width of the velocity bias zones (cf. Giddings' classification of short-range, long-range and trans-column velocity biases) [8]:

$$h_{eddy} = \sum_{j=1}^{N} h_{eddy,j} \tag{3}$$

wherein N is the number of considered scales, and wherein each $h_{eddy,j}$ consists of two contributions: one manifesting itself at very high ν (A_j), and one prevailing in the low ν_i-range (C_j). Both relate to the same transversal velocity difference (in short: "velocity bias") and are commonly accepted to interact via Giddings' famous coupling law [8,9].

$$h_{eddy,j} = \left[\frac{1}{A_j} + \frac{1}{C_j.\nu_i}\right]^{-1} \quad (4)$$

or, equivalently, via the more recently established [15]:

$$h_{eddy,j} = C\nu.\left[1 - \frac{C_j\nu_i}{2A_j}.\left(1 - e^{-2A_j/(C_j\nu_i)}\right)\right] \quad (5)$$

Although the maximal difference between the two expressions is only 12% when plotted with the same A_j and C_j-constants, Eq. (5) can be considered to be more physically sound (because it is derived directly from the advection-diffusion mass balance expressed over an elementary velocity bias zone). Another advantage of Eq. (5) over Eq. (4) is that it also rigorously holds on the trans-column scale such that all terms in Eq. (3) can be written in the same form, while Eq. (4) becomes a too crude approximation at that level and needs to be separated from the other terms, which adds to the ambiguity of the eddy dispersion definition.

The A_j- and C_j-constants appearing in Eqs. (4) and (5) are surrounded by some persistent misunderstandings. First, the C_j-constants are often confounded with the C_m and C_s in Eqs. (2b-c). These relate to the mass transfer at the single particle level, while the C_j-constants relate to the mass transfer processes over distances covering multiple particle diameters. In many literature reports, only one term is considered in Eq. (3), in which case the subscript j is commonly dropped, thus adding to the confusion with the C_m- and C_s-constants, especially considering these are often also grouped in a single term by introducing $C=C_m+C_s$. Secondly, the A_j-constant is often confounded with the total h_{eddy}-contribution, because over time the notions "A-term band broadening" and "eddy dispersion" have often been used as synonyms, which obviously they are not, since the A-contribution (or "mechanic" dispersion as referred to in the ancient literature [16]) is only a part of the eddy dispersion as is clear from Eqs. (3) and (4). More precisely, it is the part of the eddy dispersion that becomes dominant at high velocities.

One of the consequences of the erroneous use of the notions "A-term" and "eddy dispersion" as interchangeable synonyms is that the field has become infected with the idea that the eddy dispersion is independent of the zone retention factor k'' or the diffusion coefficient D_m. This idea was further instigated by the fact that Giddings in his famous coupling theory did not consider any retention effects [8,15]. Recent experimental evidence however shows that, when applying Eq. (1), the resulting h_{eddy}-values strongly depend on the analyte retention [17–19].

In [15], it has been shown that, although the A_j- and C_j-constants relate to the same velocity bias zone and both are proportional to the square of the relative velocity difference across this zone [8,15], there

96 are some distinct differences: whereas the A_j-constants relate to the axial length of the bias, the C_j-
97 constants relate to the transport across the transversal width of the bias. General expressions for A_j- and
98 C_j are given in [15], showing that, whereas the A_j-constants are independent of the analyte retention
99 (and hence represent the type of dispersion referred to in the old days as the "mechanic" or "structural"
100 dispersion [8,16]), the C_j-constants clearly depend on k'', or the diffusion coefficient D_m of the analytes.

101 The aim of the present paper is to *i)* make a clear systematic study of the eddy dispersion as defined by
102 Eq. (1) over a broad range of retention factors and *ii)* develop a simple empirical model that can be used
103 to describe the k''-dependence of the eddy dispersion. For point *ii)*, it was decided to revert to a
104 generalized form of the well-established Knox-model [20]:

105 $$h_{eddy} = A.\nu_i^{n} \quad (6)$$

106 introduced by Knox in his seminal 1969 paper as a simplified approximation to Giddings' summation of
107 coupling terms (combination of Eq. 3 with 4). Eq. 4 is difficult to apply meaningfully in practice, because
108 the different contributions to this equation are difficult to deconvolute. Since then, the so-called Knox-
109 equation has been as widely used as the more classic van Deemter-expression taught in any basic course
110 in chromatography [21], despite the fact that the A-factor and n-exponent appearing in Eq. (6) have no
111 direct physical meaning and are mere fudge factors.

112 Initially, Knox proposed using n=1/3 as the exponent in Eq. (6), but decades later [22], with much more
113 data available, he concluded that n can take on quite different values that are mostly situated in the
114 range of $0.5 \leq n \leq 1$. One of the reasons for this variability is that the value of n tends to strongly depend
115 on the range of velocities to which Eq. (6) is fitted. Nevertheless, the use of n=1/3 has become dogmatic
116 in the field and is used very often for fitting experimental data [21,23,24].

117 In the present study, data were collected on two commercial packed bed columns, one packed with
118 fully-porous (FP) and one with core-shell (CS) particles. Both were long (resp. 15 and 25 cm) and had a
119 large diameter (4.6 mm) to maximally reduce extra-column contributions to the measured peak widths.
120 We also deliberately selected a large particle size (5 μm), such that measurements could be made up to
121 very high values of the reduced velocity. Experiments were carried out during two distinct periods. In
122 the first period, measurements were carried out for zone retention factors in the range $0.7 \leq k'' \leq 13$.
123 Subsequently, nearly a year later, a second measurement campaign was run to address the range of
124 very high k'' (up to k''=122). One of the reasons for considering the latter range is because the band
125 broadening resulting from the intra-particle mass transfer resistance in this case becomes vanishingly
126 small (i.e., Eq. (2c) turns to zero when k'' tends to infinity), which in turn gives more power to any
127 determination of mobile zone mass transfer resistance and eddy dispersion. Alkylphenones were used
128 as test components to minimize the influence from any secondary retention mechanisms on band
129 broadening.

2. Experimental

2.1. Chemicals and columns

Milli-Q water was prepared in the lab using a Milli-Q gradient water purification system from Millipore (Bedford, MA, USA). HPLC grade acetonitrile (ACN) was purchased from Fisher Chemicals (Erembodegem, Belgium). Polystyrene standards (MW = 500, 2000, 3000, 10.000, 20.000, 30.000, 70.000, 150.000, 300.000, 700.000, 1.000.000 and 2.000.000), used for inverse size exclusion chromatography (ISEC), were purchased from Sigma-Aldrich (Bornem, Belgium). HPLC-grade tetrahydrofuran (THF) was from VWR (Leuven, Belgium). Acetanilide was obtained from Federa Chemicals (Metro Manila, Philippines). Propiophenone, butyrophenone, benzophenone, valerophenone, hexanophenone and octanophenone were obtained from Sigma-Aldrich (Bornem, Belgium). A core-shell column Kinetex C18 (250 × 4.6 mm, 5 µm) was obtained from Phenomenex (Utrecht, Netherlands). A fully porous column Ascentis C18 (150 × 4.6 mm, 5 µm) was purchased from Sigma-Aldrich (Bornem, Belgium).

2.2. Apparatus

All band-broadening measurements were performed on an Agilent 1290 UHPLC system (Agilent Technologies, Waldbronn, Germany) equipped with a quaternary pump, autosampler and diode array detector with a flow cell of 1 µL. Viper tubing with an i.d. of 75 µm and the shortest possible length (Thermo Scientific, Germering, Germany) was used to connect the column to the system. Chemstation software (Agilent Technologies) was used to control the UHPLC system and for data acquisition and processing. The measurements were performed at room temperature, and an injection volume of 1 µL was used. The flow rates ranged between 0.02 and 2 mL/min for the core-shell column, and between 0.02 and 2.5 mL/min for the fully porous column. The absorbance was measured at a wavelength of 210 nm.

2.3. Sample preparation

Stock solutions of acetanilide, propiophenone, butyrophenone, benzophenone, valerophenone, hexanophenone and octanophenone were prepared in a concentration of 10.000 ppm in ACN. Fresh test samples were prepared daily by mixing and diluting stock solutions until a final concentration of 500 ppm in the mobile phase used for the evaluation of the column performance (for details see Table 1).

2.4. External porosity and particle size measurement

Values of the external porosity (ε_e) for the fully porous and the core-shell column were determined experimentally via ISEC experiments [25] at a flow rate of 0.4 mL/min and using an injection volume of 1 µL. To determine the true particle size of the columns, the columns were opened after analytical measurements and the particles were removed by flushing the columns with isopropanol. The particles were subsequently dried by evaporating the isopropanol at room temperature in the fume hood and prepared for SEM measurements. The employed instrument SEM instrument was a JCM-6000 Plus

Neoscope (JEOL) with a Tungsten filament and was operated at an accelerating voltage of 5 kV and a 2200× magnification. The particles were conductive enough to omit the use of a carbon coating. Of every particle batch, 10 pictures were taken and of every batch the diameter of at least 500 particles was measured to determine the particle size distribution. To actually measure the particle sizes, the SEM pictures were analyzed with the JCM-600 Plus Version 1.6 software. Fig. S1 in the Supporting material (SM) shows representative SEM-pictures, while Fig. S2 shows the resulting normalized particle size distribution obtained for the two columns [26].

2.5. Plate height measurements

All experiments were conducted in isocratic mode. Premixed mobile phases consisting of ACN and H_2O in varying ratios were used to produce different zone retention factors (k", see Eq. (11) further on). The exact composition of the employed mobile phases can be found in Table 1, together with the actual zone retention factors and diffusion coefficients of the compounds. Diffusion coefficients were measured via the Taylor-Aris open tube method [27]. The zone retention factors given in Table 1 were determined when the columns were operated at their respective optimum velocities.

Column efficiencies (N_{col}) were determined from peak widths at 4.4% of the peak height ($w_{4.4\%}$), and corrected for the system contribution (t_{sys} and σ^2_{sys}), that was measured by removing the column from the system and replacing it by a zero dead-volume union:

$$\sigma^2 = \frac{w_{4.4\%}^2}{25} \tag{7}$$

$$N_{col} = \frac{\left(t_{total} - t_{sys}\right)^2}{\sigma^2_{total} - \sigma^2_{sys}} \tag{8}$$

$$H_{col} = \frac{L}{N_{col}} \tag{9}$$

For the least retained compound (k"= 0.67), the system contribution was always less than 5% of the overall contribution (for all flow rates on both columns), for all other compounds (k"> 0.67), the system contribution was always well below 2%.

3. Results and discussion

In what follows, all results are interpreted in terms of the zone retention factor k'', as this is the retention factor appearing in Eqs. (2a-c). In the present study, k'' was determined experimentally from the measured external porosity ε_e, the interstitial velocity u_i, the column length L, the analyte retention time t_R and the flow rate F:

$$u_i = \frac{F}{\varepsilon_e \pi r^2} \tag{10}$$

$$k'' = \frac{t_R \cdot u_i}{L} - 1 \quad (11)$$

The zone retention factor k'' is linked to the more frequently used phase retention factor k' appearing in the expression for the retention time and separation resolution via [11]:

$$k' = \frac{\varepsilon_e}{\varepsilon_T}(1 + k'') - 1 \quad (12)$$

Fig. 1 shows the reduced plate height plots as recorded for both columns (see Fig. S3 in the Supporting material (SM) for corresponding absolute plate height plots). A first observation that can be made is that the low k''-series ($k'' \leq 13$) and the high k''-series ($33 \leq k'' \leq 135$) clearly are in line with each other, despite the fact they were measured more than 10 months apart and were carried out by a different experimenter.

Both columns are clearly well-packed, as they both display a minimum plate height (h_{min}) well below 2 (resp. h_{min}=1.50 and h_{min}=1.66 for the weakliest retained analyte on the FP and the CS column). Whereas a h_{min} of 1.66 is rather average for a core-shell column, the h_{min}=1.50 for the FP-column is exceptionally low and to the best of our knowledge one of the lowest ever reported h_{min}-values for a FP particle column. Admittedly, the sub-h=2 plate heights reported here are for components with a very low zone retention factor (zone retention factor =0.7 corresponding to a phase retention factor around k'=0.2). Considering somewhat higher retention factors (k''=3.46 and k''=6.45, resp. corresponding approximately to k'=2 and k'=4), the h_{min}-values of the FP column are already at h_{min}=1.9 and 2, which is typical for a well-packed FP column [1].

At this point, it is important to note that the h- and ν_i-values reported in the present study are not simply based on the nominal particle size specified by the manufacturer (5 μm in both cases) but were calculated using the experimentally determined number-averaged d_p-value [28] that was obtained by opening the columns and measuring the actual particle size distribution using SEM images (cf. Section 2.4). This analysis showed the average particle size was d_p= 4.46 μm for the CS-column and d_p= 5.18 μm for the FP-column. The analysis also showed the particle size distribution (PSD) of the FP particles is significantly broader than for the CS particles (see Fig. S2 in SM), which is also a typical observation made when comparing CS and FP particles [3]. Hence, the exceptionally low plate heights of the FP column cannot be explained by the PSD of its particles either. It is however preferred here not to further speculate on the reasons underlying the exceptionally low h-values for the FP-column (especially when compared to the CS-column), for this is not the topic of the present study and only one column of each type has been investigated.

Returning to Fig. 1, another clear observation that can be made for both columns is that the optimal velocity ($\nu_{i,opt}$) and the corresponding h_{min} both increase with increasing zone retention factor and that this trend continues up to the highest investigated zone retention factor of $k'' \cong 120$. Undoubtedly the major factor contributing to this phenomenon is the B-term band broadening, which clearly also

strongly increases with the retention factor, as can be assessed from the strong increase of h with k'' in the low ν_i-range. As it is furthermore well-known [29] that in chromatography the optimal velocity increases with $B^{1/2}$, the shift in $\nu_{i,opt}$ with k'' is straightforward to understand. Similarly, since the simple van Deemter plate height model shows that $h_{min}= A+(B.C)^{1/2}$ [29], the increase of h_{min} with B, and hence with k'', is also obviously expected.

To investigate this further, the value of the B-term constant was determined for each of the different k''-series. As shown in [30], determining the value of B is also the first step to calculate h_{eddy} via Eq. (1). In the present study, B-term constants were determined using the curve fitting procedure described in [31]. It was shown there that this method produces B-term constants that are within 0.7% of the results obtained via peak parking experiments. The advantage of the former method is that no extra measurements are required when the van Deemter-data are anyhow available down to a sufficiently low reduced velocity (say down to ν_i=0.25). Examples of the extrapolation procedure applied to the current data sets are shown in Fig. S4 of the SM. For the higher k''-value series, the lowest reduced velocity was already as high as ν_i=5, but given the very high values of B, these could still be determined with an estimated accuracy of some 3-5%.

The resulting B-term constants are shown in Fig. 2, where the B-term constant clearly strongly increases with k''. The reason underlying this trend can be readily understood from Eq. (2a), showing that $B \propto(1+k'')$. Obviously, the effective diffusion coefficient D_{eff} slightly counteracts this dependence (hence the deviation from a perfectly straight line), as D_{eff} is known to decrease with increasing k''. However, this decrease occurs at a much slower pace than the increase originating from the (1+k'')-proportionality [32,33]. The fact that the CS-particles produce consistently lower B-values than the FP-particles is in line with all previous literature on the difference in D_{eff} between CS and FP-particles [12,32,34]. One important factor explaining this, is the presence of the core in the CS-particles which imposes an additional obstruction to the longitudinal diffusion. This effect can be calculated to lead to an approximately 10% reduction of D_{eff} [35], which is on the same order as the difference observed here.

With the known B-values, it is now straightforward to calculate the h_B-contribution needed to make the subtraction in Eq. (1). Next, applying the effective medium theory (EMT) introduced in [36] and [37], the B-values can also be used to estimate the diffusion coefficient in the porous zone of the particles (D_{pz}) needed to calculate h_{Cs} (Eq. 2c). As described in [37], this first involves calculating the so-called polarizability constant β_1, which, using a second order EMT approximation, can be calculated using:

$$\beta_1 = \frac{(\varepsilon_e - 1)(4 + B\varepsilon_e) + \sqrt{(\varepsilon_e - 1)^2(4 + B\varepsilon_e)^2 + 8\varepsilon_e\zeta_2(B\varepsilon_e - 2)^2}}{4\varepsilon_e\zeta_2(B\varepsilon_e - 2)} \qquad (13)$$

wherein ε_e is the external porosity of the bed. In the present study, ε_e was determined using the ISEC-method described in Section 2.4, showing that the FP-column had an external porosity of ε_e = 0.371 while the CS-column had ε_e = 0.412 (see Fig. S5 of the SM for a plot of the ISEC data points and read-out

of ε_e). Further, ζ_2 is the geometrical three-point parameter [36], with a value depending on the particle fraction (1-ε_e). In [35], it was found that ζ_2=0.2-0.3 is a good approximation for the typical packing density in random sphere packings. This parameter anyhow only has a secondary effect on the value of β_1. All data in the present study were calculated using ζ_2=0.3, as values close to ζ_2=0.2 led to an obvious outlier with physically impossible values for the largest k''-data point (see also discussion of Fig. 2b further on for modelling difficulties at very high k'').

From the value of β_1, the relative permeability α_{part} can be calculated using [37]:

$$\alpha_{\mathrm{part}} = \frac{1 + 2 \cdot \beta_1}{1 - \beta_1} \tag{14}$$

from which, in turn, the pursued value of D_{pz} can be readily obtained via:

$$\mathrm{D_{pz}} = \frac{2 + \rho^3}{2} \cdot \alpha_{\mathrm{part}} \cdot \frac{1 - \varepsilon_e}{\varepsilon_e k''} \cdot \mathrm{D_m} \tag{15}$$

wherein ρ is the relative core radius (ρ=0.717 according to the data supplied by the manufacturer). This procedure was applied to all B-data and led to the set of D_{pz}/D_m-data shown in Fig. 2b. As can be noted, there is no significant difference between the D_{pz}-data for the FP- and CS particles. This shows the difference in B-term observed in Fig. 2a can be fully attributed to the presence of the solid core in the CS particles (D_{pz} respectively is the effective diffusion inside the entire FP-particle or inside the shell-zone of the CS-particles).

In the low k''-range (roughly k''< 15), the D_{pz}-data cluster around D_{pz}/D_m=0.4-0.5, with some notably smaller values for the very lowest k'' (Fig. 2b). A very slight decrease can also be discerned in the range of the larger k''-values (k''> 15). Finally, D_{pz} appears to increase again somewhat at the highest k''-value, but no firm conclusions should be attached to this since the EMT theory is known [38] to become less accurate when the conductivity of the two media lies very far apart, i.e., when α>> 1 or α<< 1. Since $\alpha \propto k''$ (cf. Eq. (12) in [37]) this is indeed certainly the case for the k''= 120-data points. Anyhow, the contribution of h_{Cs} (which is the value we are eventually after when calculating D_{pz}) is extremely small at these very high k''-values, such that this potential inaccuracy becomes insignificant for the present study.

With D_{pz} known from the data in Fig. 2b, h_{Cs} can now be calculated for each of the different reduced plate height data series. With h_B also known via Fig. 2a and Eq. (2a), we are only left with the calculation of h_{Cm} in order to calculate h_{eddy} via Eq. (1). The only uncertain factor in the expression for h_{Cm} is the Sherwood-number Sh (cf. Eq. 2b). In general, Sh is a function of the reduced velocity, and a panoply of different expressions for this function exist in literature. As shown in [14], the most commonly used correlations such as the Wilson-Geankoplis, the Katoaka or the Pfeffer model [39–42] can be severely criticized for the fact that they are used far outside the range in which they were experimentally determined (the Wilson-Geankoplis correlation was established for values of ν_i well above ν_i=50, i.e.,

well above the range typically used in chromatography). One of the consequences of using these functions is that they turn to zero when ν_i turns to zero, while physical argumentation and computational fluid dynamics (CFD) simulations show this certainly should not be the case. The CFD-simulations in [14] showed that, at ν_i =4 for example, the expression most frequently used in literature, i.e., the Wilson-Geankoplis correlation, underestimates the Sh-number in a bed of spheres by a factor of four (300% error). At ν_i =32, the Wilson-Geankoplis correlation still underestimates Sh by a factor of 2.8 (180% error). To remedy this, Eq. (16) was proposed in [14] as a much more accurate representation of the local mass transfer rates in a packed bed of spheres:

$$\mathrm{Sh} = \frac{13}{1 + 2.1\,.\,\nu_i} + 8.6\,.\,\nu_i^{0.21} \qquad (16)$$

Using Eq. (16) to calculate h_{Cm}, all data are now available to calculate the eddy dispersion according to Eq. (1). The resulting data are shown in Fig. 3. Before discussing the resulting h_{eddy}-values it is, however, instructive to look at the respective contributions of the different h_B-, h_{Cm}- and h_{Cs}-terms to the total plate height, in order to have a feeling for the impact of their subtraction. This is shown in Fig. 4 for the CS column for the cases of data from low, medium and high k'' measurements. Data for the FP column are not shown for they are fully similar. As can be noted from Fig. 4, and in full agreement with physical expectations, the h_B-contribution is the dominant factor for velocities below the optimal velocity $\nu_{i,opt}$, while it rapidly drops for larger velocities. The contributions of h_{Cm} and h_{Cs} are clearly small over the entire ν_i-range (maximally 20% at the highest reduced velocity), with h_{Cm} and h_{Cs} of similar magnitude when k'' is small and with $h_{Cs} << h_{Cm}$ for the largest considered k''. This also implies the contributions of the calculated h_{Cm}- and h_{Cs}-values in the subtraction process in Eq. (1) are relatively small. In overlay (open symbols, dashed lines), Fig. 4 also shows the h_{Cm}-contribution that would be obtained when adopting the commonly used Wilson-Geankoplis correlation. Clearly the latter leads to significantly larger h_{Cm}-values, implying that in this case (pertaining to almost all previous studies in literature) a significantly larger part would be subtracted when applying Eq. (1).

Returning now to Fig. 3, it can be clearly seen that, whereas the total plate height curves in Fig. 1 clearly shift upward with increasing k'', the h_{eddy}-curves show the opposite trend. Even more, and in contrast with the widely held view that the eddy dispersion is independent of the analyte's retention (cf. Introduction), the effect of k'' is relatively strong. For the CS column for example, h_{eddy} = 1.1 at ν_i =5 for the lowest k'' (k''= 0.67), while at the same velocity h_{eddy} = 0.45 for the highest k'' (k''= 122). This is more than a factor of two smaller. The absolute difference furthermore slowly increases when the velocity increases. The relative difference on the other hand slowly decreases. At ν_i =20 for example, h_{eddy} = 1.8 for the lowest k'', while h_{eddy} = 1 for the highest k''. A similar trend is observed for the FP-column, although in this case the difference in h_{eddy} between the lowest and highest k'' is somewhat smaller, with h_{eddy} = 1 for the lowest k'' and h_{eddy} = 0.5 for the highest k'' at ν_i =5. At ν_i =20, h_{eddy} drops from h_{eddy} = 1.6 for the lowest k'' to h_{eddy} = 1 for the highest k''.

As a side note, and bearing in mind that the h_{eddy}-values are based on the true particle diameter (experimentally determined via SEM) and not on the nominal value, it is striking to see that the FP column produces eddy dispersion values that are similar and even slightly smaller than the CS-column (compare data in Fig. 3a with Fig. 3b). This is unexpected as most studies described in the literature and in our lab showed that the eddy dispersion in core-shell columns is significantly smaller in CS- than in FP-columns [12,34,43]. However, we believe no significant conclusions should be drawn from the present finding, as the two tested columns are not from the same manufacturer and only one column of each type was investigated. The only firm comment that can be made is that the FP-column appears to be exceptionally well packed, while the CS-column is relatively speaking less well-packed (see also discussion of Fig. 1).

The final step in our study is aimed at building a simple and directly applicable model to represent and predict the eddy dispersion in packed bed columns as a function of the velocity as well as the retention coefficient. As mentioned in the introduction, a generalization of the simple Knox-model (Eq. 6) was selected for this purpose. This model assumes the data display a power-law dependence. To verify this, it is most convenient to switch to logarithmic axis. This is done in Fig. 5, confirming the h_{eddy}-data points indeed closely follow a straight-line relationship in log-log coordinates, thus validating the use of a power-law model. It is also interesting to note that the slope of the curves (corresponding to the value of n in Eq. 6) steepens with increasing retention factor, at least for the lowest k''-values. This trend is apparent on both the CS- and the FP-column. To study this in more detail, the actual best-fit A- and n-values and the corresponding R^2-values are listed in Table 2. The correlation with k'' is also graphically represented in Fig. 6. As can be noted from the agreement between the full line curves and the experimental data points in Fig. 3, as well as from the R^2-values in Table 2 (most larger than R^2=0.990, with R^2=0.946 the lowest value), the power-law model described by Eq. (6) fits the data rather well, especially considering the experimental data are inevitably impacted by measurement errors.

Apart from some fluctuations, the data in Fig. 6 display a clear relationship the best-fit A- and n-constants and the retention factor. This relationship is very similar for the CS- and the FP-column. In agreement with the gradual variation in slope observed in Fig. 5, the best-fit n-values increase with k'' for the lowest values of k'' and then level off to some value around n=0.5 for k''>10, with an exception for the small overshoot up to n=0.57 around k''=10. For the lowest value of k'' (k''=0.7), it is found that n=0.35 and n=0.4 on the CS- and the FP-columns, respectively. These values lie close to the original n=1/3 value proposed by Knox. The n-values around n=0.5 obtained for the highest k'' are of the same order as those proposed by Knox in his 2002 paper [22]. The values of A show an opposite trend. Below k''$\cong$ 10, the value of A decreases steeply with increasing k'' while this decrease levels off above k''$\cong$ 10. Around k''= 10, the FP-column data cluster around an apparent local minimum. At present, we prefer not to over-interpret the appearance of the intermediate maximum (n-data) or minimum (A-data) appearing in Fig. 6a and 6b as there are many possible explanations for the potentially incidental nature

of this observation: small secondary differences in band broadening behavior depending on the nature of the components, A and n are not entirely independent which can lead to fitting errors, etc. Hence, ignoring these local extrema, and keeping to a 3-parameter expression to model the data in Fig. 6, the following fitting function expressions were obtained:

$$n = 0.55 - 0.26 \,.\, k''^{-0.45} \tag{17}$$

$$A = 0.19 + 0.12 . k''^{-0.93} \tag{18}$$

If desired, Eq. (12) can be used to express Eqs. (17)-(18) as a function of the more customarily used phase retention factor k' instead of k''. Please note the constants in Eqs. (17)-(18) are plain fudge factors and have no physical meaning whatsoever. Furthermore, it can also be expected the fitting constants will vary depending on the packing quality of the columns because different packing qualities can obviously be expected to lead to a different h_{eddy}, in turn inevitably requiring a different A and (to a lesser extent) n to represent it.

Despite the frequently claimed lack of a direct and clear physical meaning for the A- and n-parameters, it is believed the overall trends observed for the A -and n-constants in Fig. 6 are, at least qualitatively, generalizable to any other packed bed chromatography column, because these trends can be clearly rationalized via the physical meaning of the A_j- and C_j-constants appearing in the local scale $h_{eddy,j}$-models (cf. Eqs. 4-5). This can be understood from the dependence of these constants on k'', which has been mathematically derived in [15]. It was shown there that, whatever the velocity bias scale included in Eq. (3) and save the secondary effect of the zone retention factor on the transversal dispersion, the C_j-constants vary inversely proportional with (1+k'') and hence decrease with increasing k''. As a consequence, the transition velocity [8,22] at which the h_{eddy}-curve described by Eq. (4) or (5) switches from a linear increase (C-term dominated behavior, n=1) to a saturated value (A-term dominated behavior, n=0) shifts to ever larger velocities when k'' increases. This implies that progressively larger parts of the velocity range can be expected to appear C_j-dominated with increasing k''. Since h_{eddy} in this regime essentially varies linearly with ν_i (save for a minor effect originating from the velocity-dependence of the transversal dispersion), it is hence evident that in this case the n-power in Eq. (6) will tend to n=1. Conversely, when C_j is large (i.e., for small k''), h_{eddy} will initially rise very steeply with ν_i but will then remain constant at h_{eddy}=A for the rest of the ν_i-range. It is in this case obvious to expect that the power of the ν_i-dependency will rather tend to zero (to more closely represent the saturating nature of the h_{eddy}-curve). On the other hand, the A-constant appearing in Eq. (6) can be considered a measure for the absolute magnitude of both the A_j and C_j-components. The fact that A decreases with increasing k'' in Fig. 6 can then again be understood from the fact that the C_j-components of the eddy dispersion decrease with increasing k''.

The above explanation can also be used to attribute a physical meaning to the n- and A-constants in Eq. (6), in the sense that n can be regarded as a measure for the relative dominance of the C_j-component:

the closer n gets to unity, the more h_{eddy} is dominated by a C_j-term type of eddy dispersion (i.e., the type of dispersion where h_{eddy} varies linearly with ν_i). The latter is connected to velocity bias zones that are long and narrow, such that there is sufficient time to reach the long-time limit dispersion regime over the length of each bias zone [15]. On the other hand, when n is low, the eddy dispersion is more dominated by its A_j-components, which is representative for the occurrence of velocity bias zones that are short and wide [15]). In turn, the A-constant appearing in Eq. (6) can be considered as a measure for the absolute magnitude of the A_j and C_j-component. Since both are depending on the square of the relative velocity difference across the transversal velocity bias marking a given considered scale, the physical meaning of the A-constant can be directly linked to the latter.

Important to note further is that, given the aforementioned importance of the transition-velocity, it is evident that the fitting of a set of dispersion data with Eq. (6) can be expected to produce slightly different A- and n-values, depending on the width of the velocity range over which the fitting is made. Obviously, this is a limitation of fitting correlations such as Eq. (6) and implies the correlation is only applicable over the range of velocities across which it has been determined.

Combining Eqs. (17) and (18) with Eq. (6), a complete model is now available that can be used to express the dependency of the eddy dispersion h_{eddy} on the mobile phase velocity u_i and the particle size, as well as on the D_{mol} and k'' of the analytes. Obviously, the fitting factors in Eqs. (17)-(18) will have to be adapted depending on the column's packing quality, with the values for A most probably more sensitive to the packing quality than the n-exponent.

4. Conclusions

Using experimental plate height measurements obtained over a very broad range of retention factors (ranging from k''= 0.7 to k''=122), it was found that the eddy dispersion band broadening gradually decreases with increasing retention factor, in contrast with the widely held view of the eddy dispersion as a contribution to h that is independent of the analyte type and only depends on the bed structure. Our finding confirms earlier observations made using the Wilson-Geankoplis model to calculate the Sherwood-number needed to determine h_{Cm} in Eq. (1). Whereas the Wilson-Geankoplis model can be expected to exaggerate the effect of k'' on h_{eddy} (it predicts a larger h_{Cm}-contribution to be subtracted from the overall h), the current Sh-model still leads to a difference on the order of some 0.5 up to 0.8 reduced plate height units between the lowest and the highest retention factor. This difference was very similar on both of the columns investigated in this work.

The widely used power-law Knox model (Eq. 6) satisfactorily fits the h_{eddy}-curves for the different k''-data series (most R^2-values larger than R^2=0.990, with R^2=0.946 the lowest value) and can be extended with two empirical expressions of the type given by Eqs. (17) and (18) to express the dependence of the A- and n-parameters on the zone retention factor. An important moderating remark is that these A- and n-values (and the quality of the fit with Eq. (6) itself) can be expected to depend on the packing quality of

the column, as well as on the velocity range over which the fit has been made, as there is no direct quantitative relationship between the A- and n-constants in Eq. (6) and the many A_j and C_j-influences contributing to h_{eddy} via Eq. (3).

The qualitative trend observed for the A- and n-constants obtained from the data for both columns (n initially increases rather steeply with k'' for low values of k'' and then goes to a plateau for k''> 10 while the A-constant decreases with increasing k'' before tending to a constant value) can be inferred to be generalizable to any other packed-bed column as this trend can be rationalized based on the effect of k'' on the C_j-constants appearing in the local scale $h_{eddy,j}$-models (cf. Eqs. 4-5). This explanation can also be used to attribute a physical meaning to the n- and A-constants in Eq. (6).

Acknowledgements

HS is funded by the Research Foundation Flanders (FWO) (post-doctoral grant No. 12Y9818N).
GD and DC acknowledge an FWO-FRNS grant EOS nr. 30897864.

References

[1] J.H. Knox, Band dispersion in chromatography – a new view of A -term dispersion, J. Chromatogr. A. 831 (1999) 3–15.

[2] F. Gritti, A stochastic view on column efficiency, J. Chromatogr. A. 1540 (2018) 55–67. doi:10.1016/j.chroma.2018.02.005.

[3] M. Catani, O.H. Ismail, A. Cavazzini, A. Ciogli, C. Villani, L. Pasti, C. Bergantin, D. Cabooter, G. Desmet, F. Gasparrini, D.S. Bell, Rationale behind the optimum efficiency of columns packed with new 1.9 μm fully porous particles of narrow particle size distribution, J. Chromatogr. A. 1454 (2016) 78–85. doi:10.1016/j.chroma.2016.05.037.

[4] R.A. Shalliker, H. Ritchie, Segmented flow and curtain flow chromatography: Overcoming the wall effect and heterogeneous bed structures, J. Chromatogr. A. 1335 (2014) 122–135. doi:10.1016/j.chroma.2013.08.004.

[5] S. Bruns, J.P. Grinias, L.E. Blue, J.W. Jorgenson, U. Tallarek, Morphology and separation efficiency of low-aspect-ratio capillary ultrahigh pressure liquid chromatography columns, Anal. Chem. 84 (2012) 4496–4503. doi:10.1021/ac300326k.

[6] S. Bruns, E.G. Franklin, J.P. Grinias, J.M. Godinho, J.W. Jorgenson, U. Tallarek, Slurry concentration effects on the bed morphology and separation efficiency of capillaries packed with sub-2μm particles, J. Chromatogr. A. 1318 (2013) 189–197. doi:10.1016/j.chroma.2013.10.017.

[7] F. Gritti, G. Guiochon, Perspectives on the evolution of the column efficiency in liquid chromatography, Anal. Chem. 85 (2013) 3017–3035. doi:10.1021/ac3033307.

[8] C. Giddings, Dynamics of Chromatography: Principles and Theory, New York, 1965.

[9] F. Gritti, G. Guiochon, Perspectives on the evolution of the column efficiency in liquid chromatography, Anal. Chem. 85 (2013) 3017–3035. doi:10.1021/ac3033307.

[10] I. Bacskay, A. Felinger, Macroscopic and microscopic analysis of mass transfer in reversed phase liquid chromatography, J. Chromatogr. A. 1216 (2009) 1253–1262. doi:10.1016/j.chroma.2008.11.054.
[11] G. Desmet, K. Broeckhoven, Equivalence of the different Cm- and Cs- term expressions used in liquid chromatography and a geometrical model uniting them, Anal. Chem. 80 (2008) 8076–8088.
[12] F. Gritti, G. Guiochon, Speed-resolution properties of columns packed with new 4.6µm Kinetex-C18 core-shell particles, J. Chromatogr. A. 1280 (2013) 35–50. doi:10.1016/j.chroma.2013.01.022.
[13] H. Song, G. Desmet, D. Cabooter, Evaluation of the Kinetic Performance Differences between Hydrophilic-Interaction Liquid Chromatography and Reversed-Phase Liquid Chromatography under Conditions of Identical Packing Structure, Anal. Chem. 87 (2015). doi:10.1021/acs.analchem.5b03697.
[14] S. Deridder, G. Desmet, New insights in the velocity dependency of the external mass transfer coefficient in 2D and 3D porous media for liquid chromatography, J. Chromatogr. A. 1227 (2012) 194–202. doi:10.1016/j.chroma.2012.01.007.
[15] G. Desmet, A finite parallel zone model to interpret and extend Giddings' coupling theory for the eddy-dispersion in porous chromatographic media, J. Chromatogr. A. 1314 (2013) 124–137. doi:10.1016/j.chroma.2013.09.016.
[16] P.G. Saffman, A theory of dispersion in a porous medium, J. Fluid Mech. 6 (1959) 321–349.
[17] D. Cabooter, H. Song, G. Desmet, C. To, C. To, HILIC and RPLC Assessment of individual mass transfer phenomena in HILIC and RPLC, Chrom+food Forum. 9 (2017) 12–14.
[18] F. Gritti, G. Guiochon, Comparison between the intra-particle diffusivity in the hydrophilic interaction chromatography and reversed phase liquid chromatography modes. Impact on the column efficiency, J. Chromatogr. A. 1297 (2013) 85–95. doi:10.1016/j.chroma.2013.04.055.
[19] F. Gritti, G. Guiochon, The rationale for the optimum efficiency of columns packed with new 1.9µm fully porous Titan-C18 particles-A detailed investigation of the intra-particle diffusivity, J. Chromatogr. A. 1355 (2014) 164–178. doi:10.1016/j.chroma.2014.05.076.
[20] J.H. Knox, J.F. Parcher, Effect of the column to particle diameter ratio on the dispersion of unsorbed solutes in chromatography, Anal. Chem. 41 (1969) 1599.
[21] U.D. Neue, HPLC Columns: Theory, Technology and Practice, Wiley-VCH, New York, 1997.
[22] J.H. Knox, Band dispersion in chromatography — a universal expression for the contribution from the mobile zone, J. Chromatogr. 960 (2002) 7–18.
[23] L. Kirkup, M. Foot, M. Mulholland, Comparison of equations describing band broadening in high-performance liquid chromatography, J. Chromatogr. A. 1030 (2004) 25–31. doi:10.1016/j.chroma.2003.11.028.
[24] S. Fekete, D. Guillarme, Kinetic evaluation of new generation of column packed with 1.3 µm core-shell particles, J. Chromatogr. A. 1308 (2013) 104–113. doi:10.1016/j.chroma.2013.08.008.

[25] H. Guan, G. Guiochon, Study of Physico-chemical properties of some packing materials. I Measurements od the external porosity of packed columns by inverswe size-exclusion chromatography., J. Chromatogr. A. 731 (1996) 27–40.
[26] D. Cabooter, J. Billen, H. Terryn, F. Lynen, P. Sandra, G. Desmet, Kinetic plot and particle size distribution analysis to discuss the performance limits of sub-2 microm and supra-2 microm particle columns., J. Chromatogr. A. 1204 (2008) 1–10. doi:10.1016/j.chroma.2008.07.007.
[27] H. Song, Y. Vanderheyden, E. Adams, G. Desmet, D. Cabooter, Extensive database of liquid phase diffusion coefficients of some frequently used test molecules in reversed-phase liquid chromatography and hydrophilic interaction liquid chromatography, J. Chromatogr. A. 1455 (2016) 102–112. doi:10.1016/j.chroma.2016.05.054.
[28] D. Cabooter, J. Billen, H. Terryn, F. Lynen, P. Sandra, G. Desmet, Detailed characterisation of the flow resistance of commercial sub-2 ??m reversed-phase columns, J. Chromatogr. A. 1178 (2008) 108–117.
[29] E. Katz, L. Ogan, R.P. Scott, Liquid Chromatography Column Design, J. Chromatogr. 289 (1984) 65–83.
[30] A. Andrés, K. Broeckhoven, G. Desmet, Methods for the experimental characterization and analysis of the efficiency and speed of chromatographic columns: A step-by-step tutorial, Anal. Chim. Acta. 894 (2015) 20–34. doi:10.1016/j.aca.2015.08.030.
[31] H. Song, D. Sadriaj, G. Desmet, D. Cabooter, Methodologies to determine b-term coefficients revisited, J. Chromatogr. A. 1532 (2018). doi:10.1016/j.chroma.2017.11.070.
[32] A. Liekens, J. Denayer, G. Desmet, Experimental investigation of the difference in B-term dominated band broadening between fully porous and porous-shell particles for liquid chromatography using the Effective Medium Theory, J. Chromatogr. A. 1218 (2011) 4406–4416. doi:10.1016/j.chroma.2011.05.018.
[33] H. Song, G. Desmet, D. Cabooter, Assessment of intra-particle diffusion in hydrophilic interaction liquid chromatography and reversed-phase liquid chromatography under conditions of identical packing structure, J. Chromatogr. A. (2017). doi:10.1016/j.chroma.2017.06.068.
[34] F. Gritti, G. Guiochon, Facts and Legends on Columns Packed with Sub-3-µm Core-Shell Particles, LCGC North Am. 30 (2012) 1–7.
[35] S. Deridder, G. Desmet, Effective medium theory expressions for the effective diffusion in chromatographic beds filled with porous, non-porous and porous-shell particles and cylinders. Part II: Numerical verification and quantitative effect of solid core on expected B-term band , J. Chromatogr. A. 1218 (2011) 46–56. doi:10.1016/j.chroma.2010.10.086.
[36] G. Desmet, K. Broeckhoven, J. De Smet, S. Deridder, G. V. Baron, P. Gzil, Errors involved in the existing B-term expressions for the longitudinal diffusion in fully porous chromatographic media. Part I: Computational data in ordered pillar arrays and effective medium theory, J. Chromatogr. A. 1188 (2008) 171–188. doi:10.1016/j.chroma.2008.02.018.

[37] G. Desmet, S. Deridder, Effective medium theory expressions for the effective diffusion in chromatographic beds filled with porous, non-porous and porous-shell particles and cylinders. Part I: Theory, J. Chromatogr. A. 1218 (2011) 32–45. doi:10.1016/j.chroma.2010.10.087.

[38] S. Torquato, Random Heterogeneous Materials, Springer Science & Business Media, New York, 2002.

[39] E.J. Wilson, C.J. Geankoplis, Liquid Mass Transfer at Very Low Reynolds Numbers in Packed Beds, Ind. Eng. Chem. Fundam. 5 (1966) 9–14.

[40] T. Kataoka, H. Yoshida, K. Ueyama, Mass transfer in laminar region between liquid and packing material surface in the packed bed, J. Chem. Eng. Jpn. 5 (1972).

[41] R. Pfeffer, Heat and mass transport in multiparticle systems, Ind. Eng. Chem. Fundam. 3 (1964) 380–383.

[42] F. Gritti, G. Guiochon, A protocol for the measurement of all the parameters of the mass transfer kinetics in columns used in liquid chromatography, J. Chromatogr. A. 1217 (2010) 5137–5151. doi:10.1016/j.chroma.2010.06.016.

[43] D. Cabooter, A. Fanigliulo, G. Bellazzi, B. Allieri, A. Rottigni, G. Desmet, Relationship between the particle size distribution of commercial fully porous and superficially porous high-performance liquid chromatography column packings and their chromatographic performance, J. Chromatogr. A. 1217 (2010). doi:10.1016/j.chroma.2010.09.008.

Figure Captions

Figure 1: Reduced plate height curves of reduced plate height (h) versus reduced interstitial velocity (ν_i) on **(a)** the core-shell and **(b)** the fully-porous particle column for alkylphenones with different zone retention factors (k") ranging between k"= 0.7 and k"= 123: ● acetanilide (k"~0.7), ■ acetanilide (k"~1.2), ◆ propiophenone (k"~3.5), ▲ butyrophenone (k"~5-6), × benzophenone (k"~7.8), ∗ valerophenone (k"~9-11), ○ hexanophenone (k"~12), □ hexanophenone (k"~34-35), ◇ octanophenone (k"~65), △ octanophenone (k"~120).

Figure 2: Plots of **(a)** B versus k" and **(b**) D_{pz}/D_m versus k" for the (○) core-shell particle and the (■) fully-porous particle column.

Figure 3: Plots of $h_{eddy}=h-h_b-h_{cm}-h_{cs}$ versus reduced interstitial velocity (ν_i) on **(a)** the core-shell and **(b)** the fully porous column for alkylphenones with different zone retention factors (k") ranging between k"= 0.7 and k"= 123: ● acetanilide (k"~0.7), ■ acetanilide (k"~1.2), ◆ propiophenone (k"~3.5), ▲ butyrophenone (k"~5-6), × benzophenone (k"~7.8), ∗ valerophenone (k"~9-11), ○ hexanophenone (k"~12), □ hexanophenone (k"~34-35), ◇ octanophenone (k"~65), △ octanophenone (k"~120). Full line curves are best-fit curves with Eq. (6). See Table 2 for fitting parameter and R^2-values.

Figure 4: Plot of relative contributions of h_b (●), h_{Cm} (▲) and h_{Cs} (◆) to the overall plate height h (■) on the core-shell column for **(a)** k"=1.2, **(b)** k"=12 and (c) k"= 122. Dashed line (△): h_{Cm} calculated via the Wilson-Geankoplis expression [10] instead of the more accurate Eq. (16).

Figure 5: Representation of h_{eddy}-data in Fig. 3 in log-log coordinates for **(a)** the core-shell and **(b)** the fully porous column. Same legend as Fig. 3.

Figure 6: Plots of the fitting factors of Eq. (6) for the (○) core-shell particle and the (■) fully-porous particle column. **(a)** n versus k" and **(b)** A versus k".

Table 1. Composition of the mobile phases and samples resp. used for the core-shell column and the fully porous column. Details on column dimensions and stationary phases are shown. Corresponding zone retention factors (k'', see Eq. 11) and diffusion coefficients, measured via the Taylor-Aris open tube method [22], are given as well.

Column	Core shell column			Fully porous column		
Compound	Mobile phase (ACN/H_2O) (v/v)	D_{mol} ($\times 10^{-9}$ m²/s)	k''	Mobile phase (ACN/H_2O) (v/v)	D_{mol} ($\times 10^{-9}$ m²/s)	k''
Acetanilide	50/50	1.01	0.67	80/20	1.57	0.68
Acetanilide	35/65	0.86	1.21	50/50	0.98	1.17
Propiophenone	46/54	1.06	3.56	60/40	1.30	3.41
Butyrophenone	46/54	0.97	6.06	50/50	1.11	5.36
Benzophenone	46/54	0.88	7.77	45/55	1.03	7.76
Valerophenone	46/54	0.89	10.59	50/50	1.00	8.92
Hexanophenone	50/50	0.91	11.93	60/40	1.07	12.63
Hexanophenone	40/60	0.74	33.63	47/53	0.83	35.17
Octanophenone	44.25/55.75	0.69	65.52	52/48	0.80	65.21
Octanophenone	40/60	0.64	122.83	47/53	0.73	114.79

Table 2. Best-fit A- and n-values and corresponding R^2-values obtained by fitting the h_{eddy} vs. ν_i data in log-log coordinates (cf. Fig. 5) to a power-law model.

Core-shell column				Fully porous column			
k″	A	n	R^2	k″	A	n	R^2
0.67	0.613	0.354	0.999	0.68	0.491	0.407	0.998
1.21	0.550	0.397	0.999	1.17	0.442	0.411	0.991
3.56	0.410	0.480	0.998	3.41	0.321	0.521	0.999
6.06	0.325	0.543	0.970	5.36	0.282	0.512	0.997
7.77	0.305	0.560	0.969	7.76	0.233	0.575	0.998
10.59	0.291	0.546	0.954	8.92	0.226	0.565	0.995
11.93	0.287	0.560	0.979	12.63	0.239	0.578	0.998
33.63	0.268	0.509	0.990	35.17	0.261	0.513	0.956
65.52	0.265	0.515	0.984	65.21	0.247	0.497	0.987
122.83	0.222	0.521	0.969	114.79	0.183	0.574	0.946

Figure 1

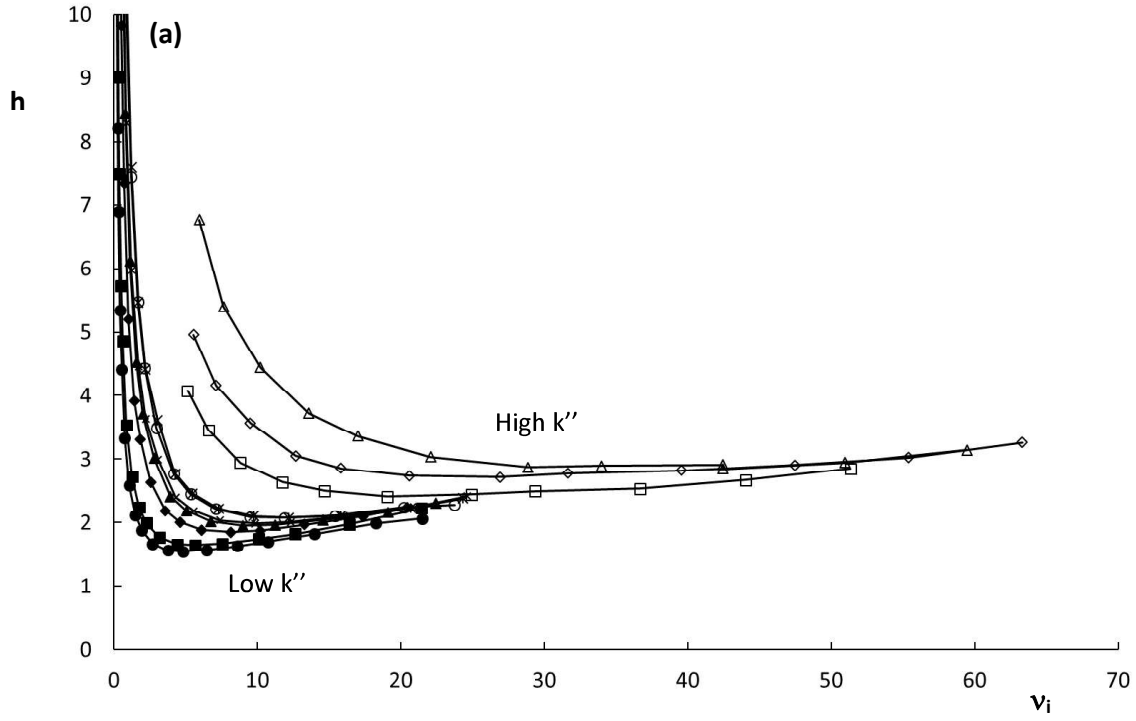

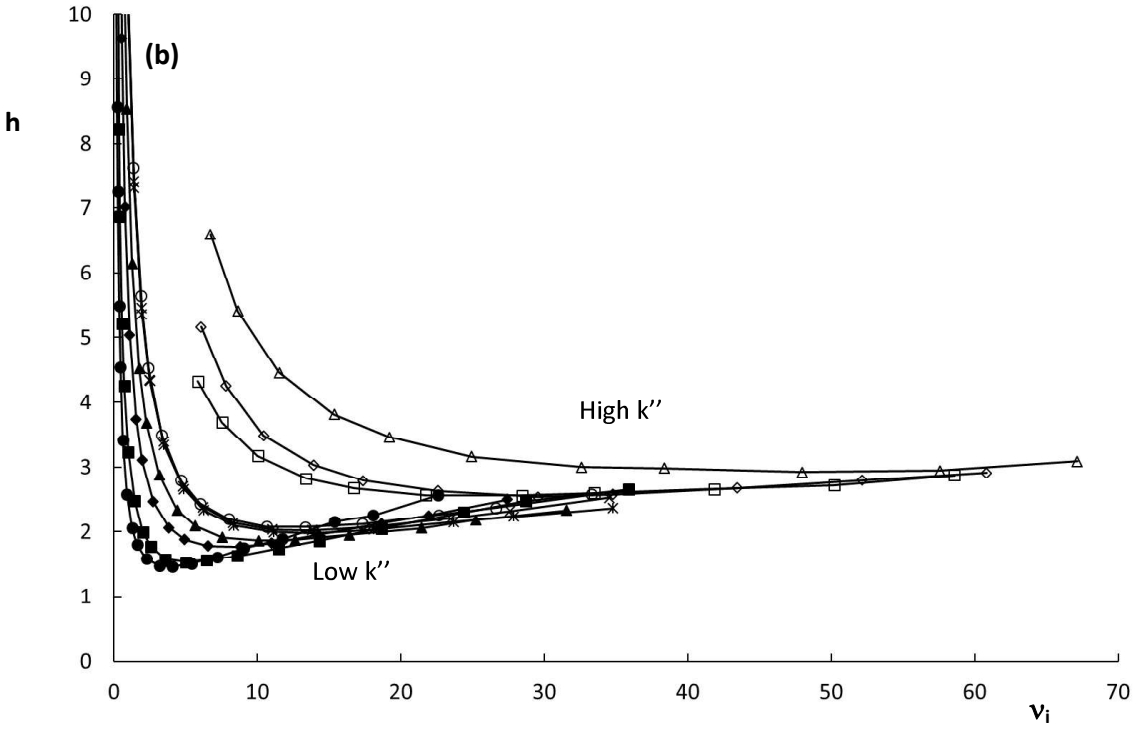

Figure 1

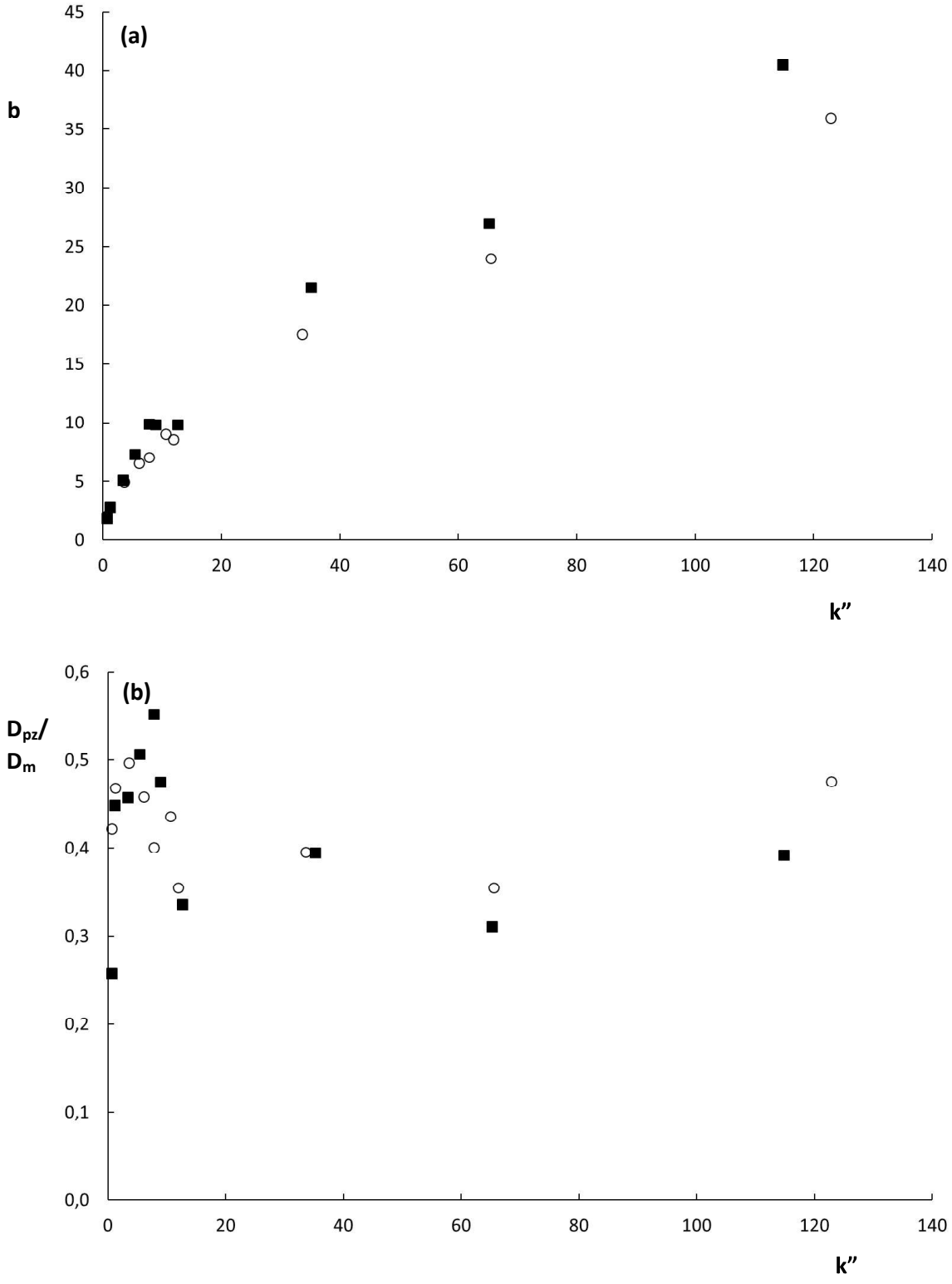
(a)
b
45
40
35
30
25
20
15
10
5
0
0
20
40
60
80
100
120
140
k”
(b)
D_{pz}/D_m
0,6
0,5
0,4
0,3
0,2
0,1
0,0
0
20
40
60
80
100
120
140
k”

Figure 2

Figure 3

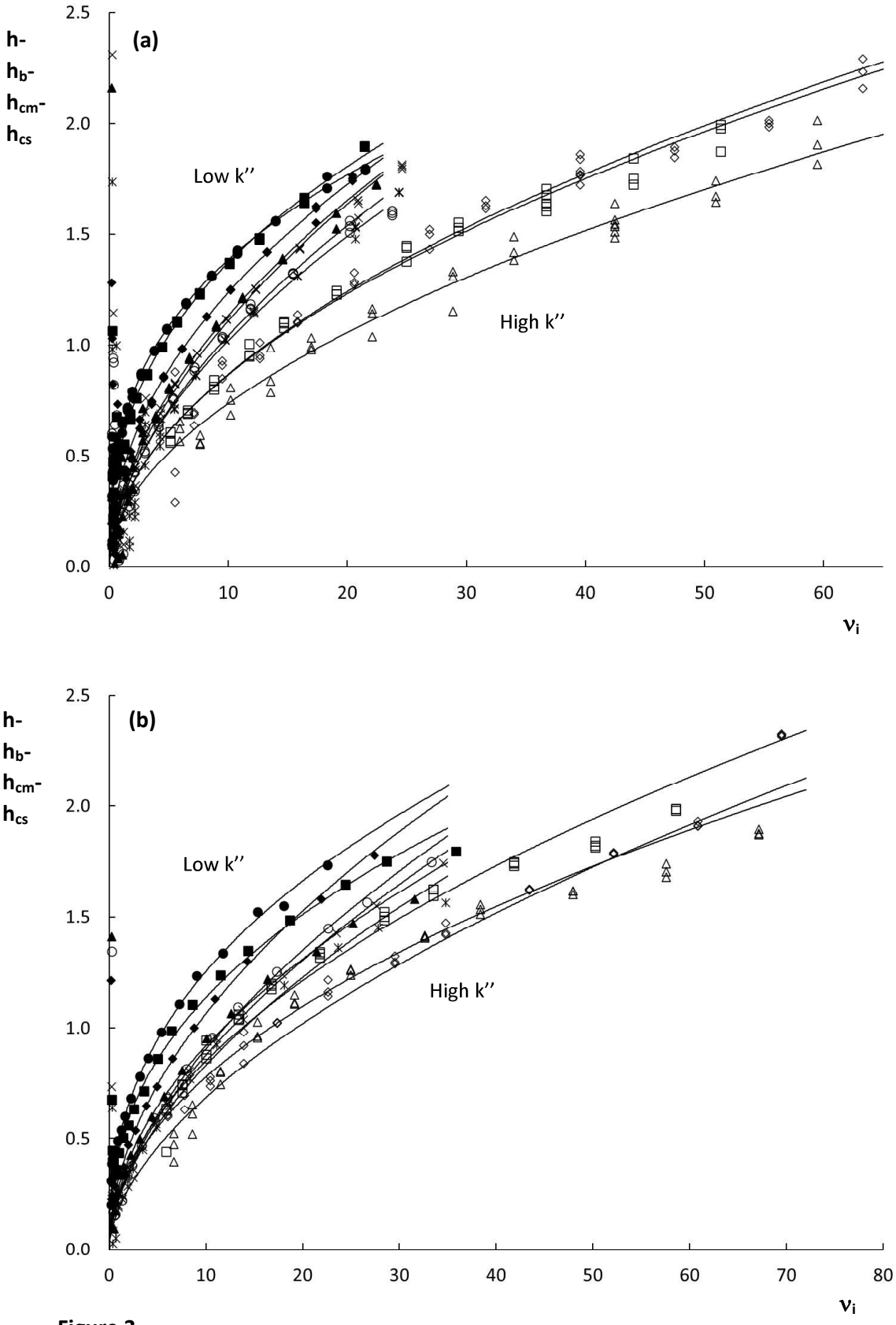

Figure 3

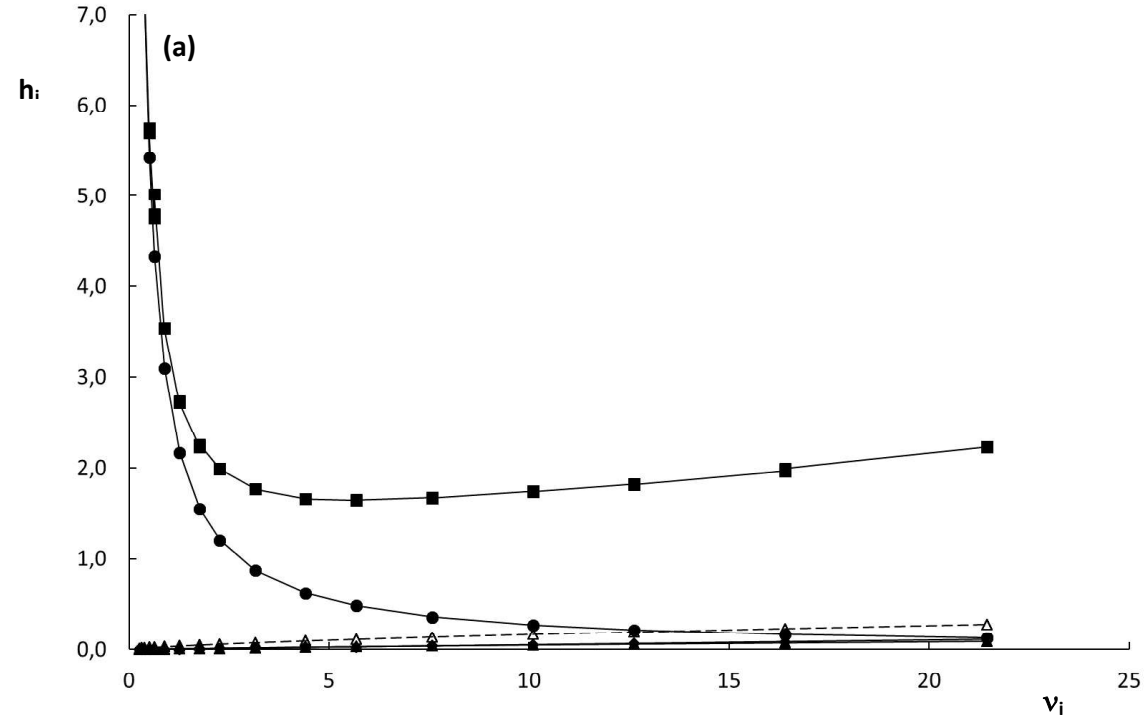
(a)
hᵢ
7,0
6,0
5,0
4,0
3,0
2,0
1,0
0,0
0
5
10
15
20
25
νi

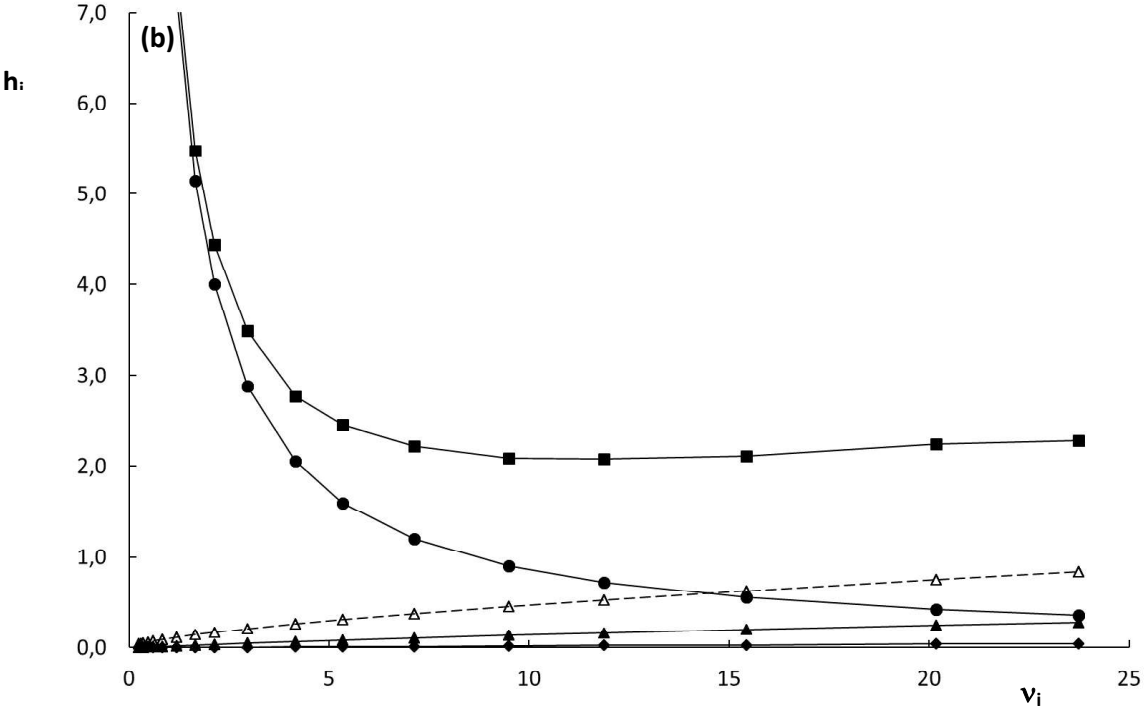
(b)
hᵢ
7,0
6,0
5,0
4,0
3,0
2,0
1,0
0,0
0
5
10
15
20
25
νi

Figure 4

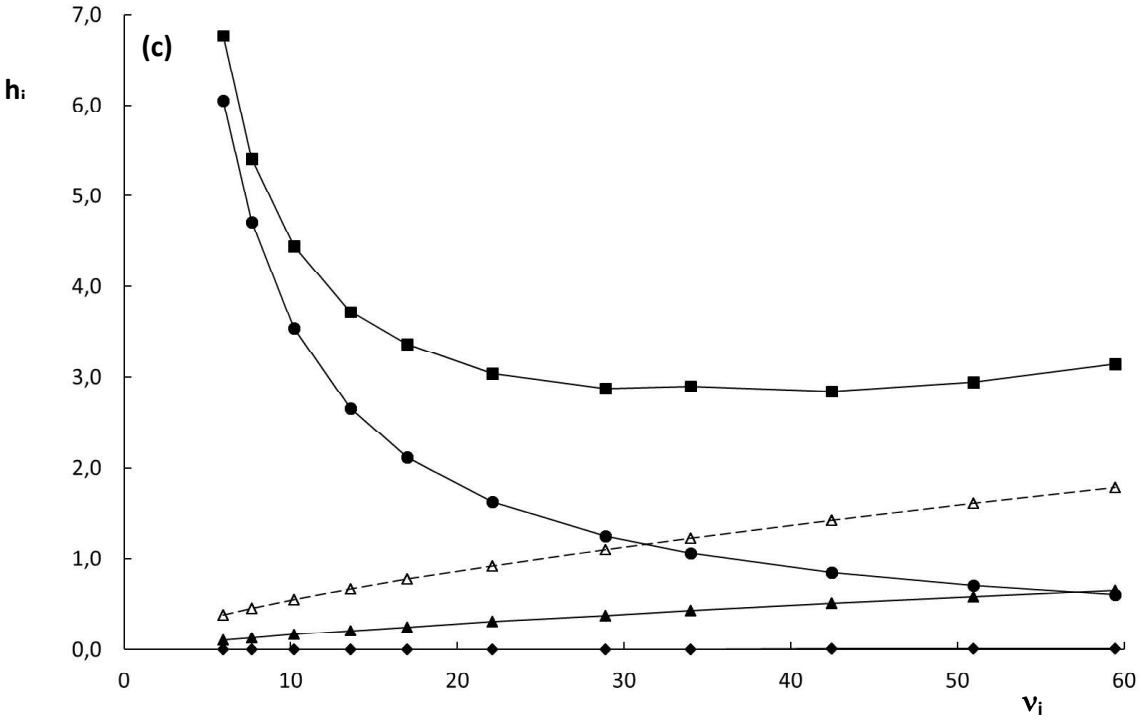

Figure 4, continued

Figure 5

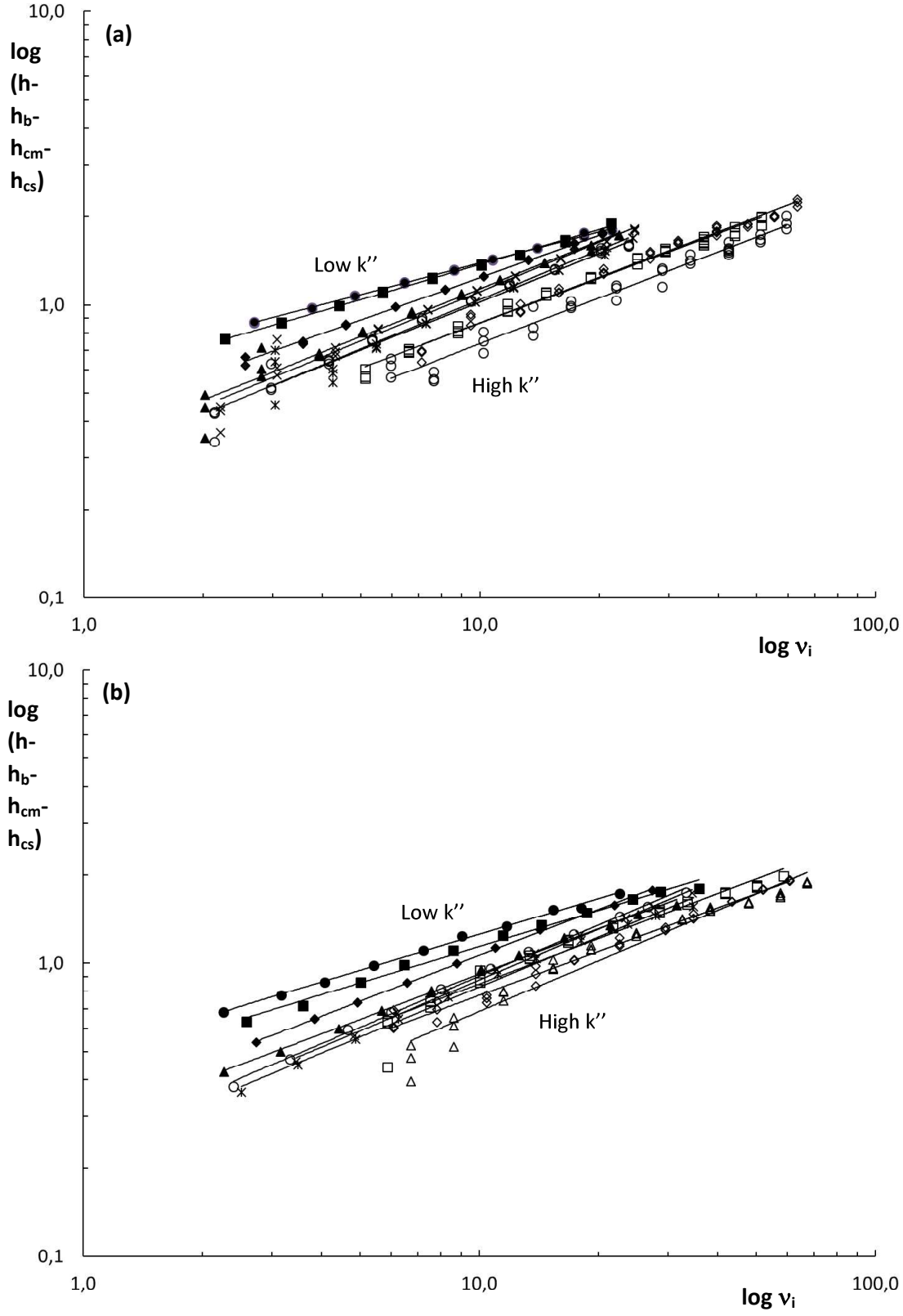

Figure 5

Figure 6

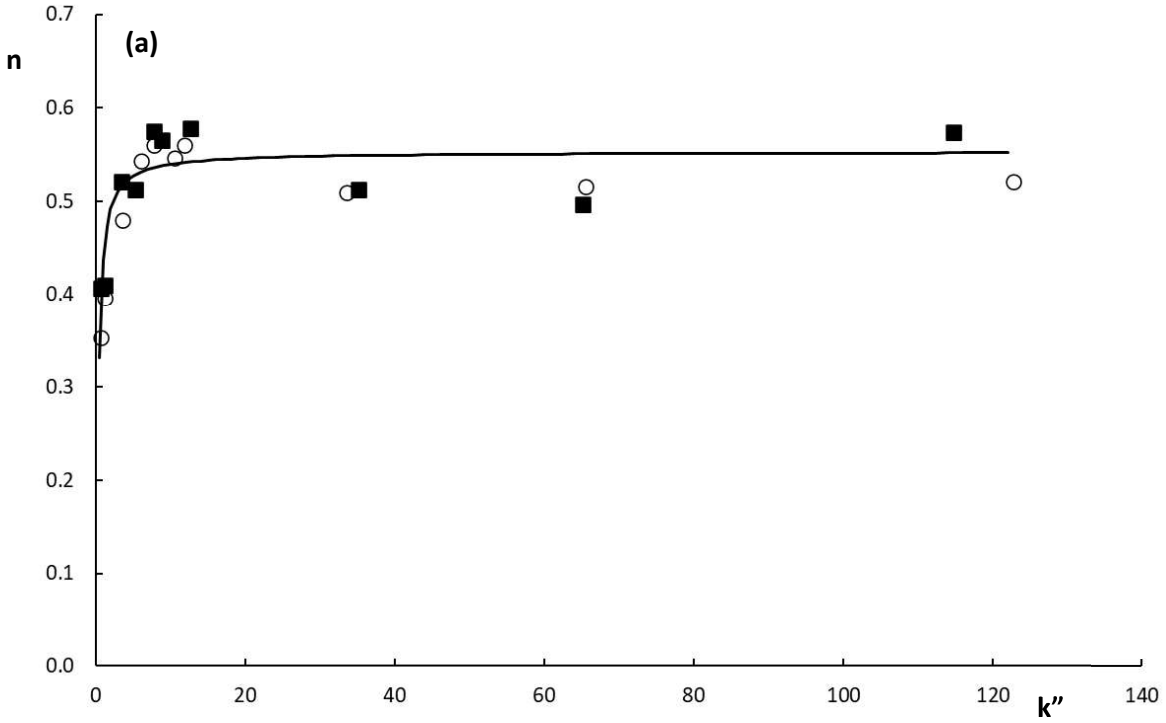

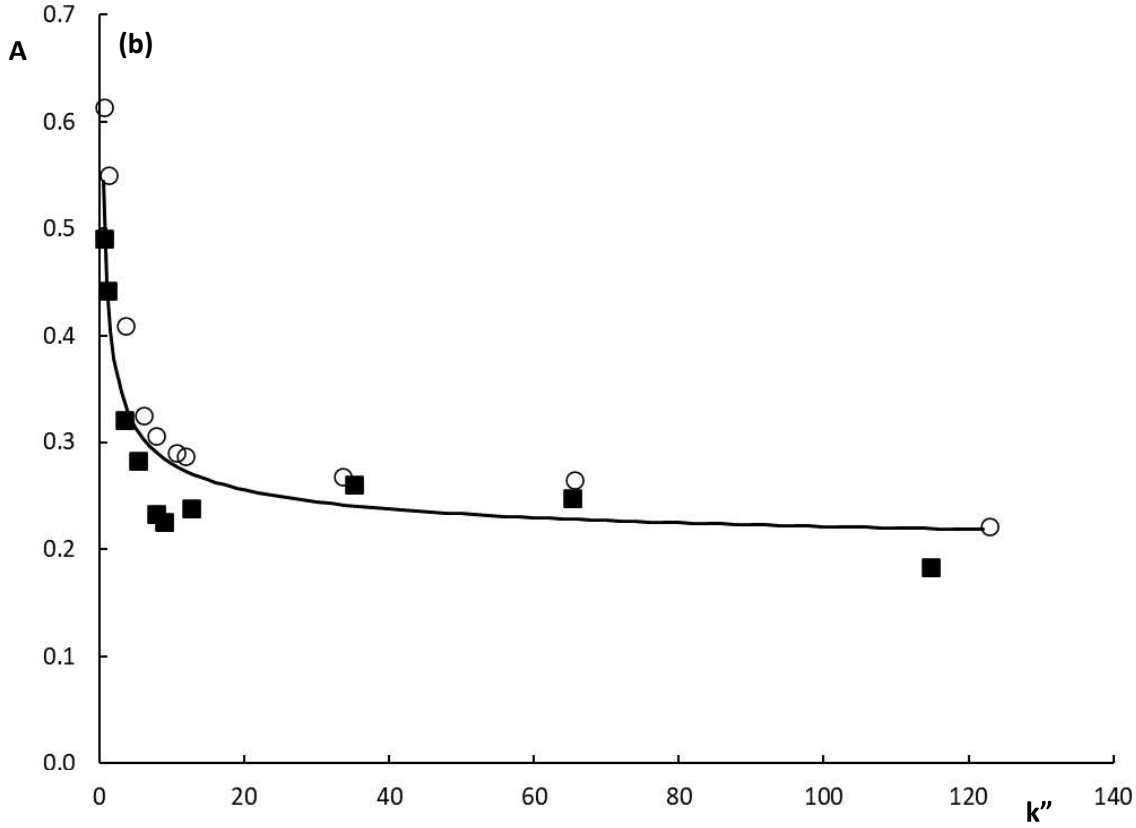

Figure 6